

Effects of Al_2O_3 Particle on Convective and Radiative Heat Flux to Rocket Base Surface

June Woo Lee*, Jae Gwan Kim* and Kyu Hong Kim*
Corresponding author: aerocfd1@snu.ac.kr

* Seoul National University, Republic of Korea

Abstract: An exhausted plume of rocket transfers a lot of heat to rocket base surface. The effects of Al_2O_3 particles and radiation heat transfer of plume are considered to study the heat flux to the base surface. Non-equilibrium 2D-axisymmetric Navier-Stokes equation with $k\omega$ -SST turbulent model is solved in the numerical analysis. As a radiation heat transfer model, P-1 radiation model is employed. In addition, the following parameters are considered which affect heat flux to rocket base surface: absorption coefficient, particle size and flight altitude. The radiative heat flux is increased as the size of particle is decreased and the absorption coefficient is increased, on the other hand, it is less sensitive to flight altitude

Keywords: Heat Flux, P-1 Radiation Model, Rocket Base Surface, Plume, Al_2O_3 particle

1 Introduction

The plume which is exhausted from the launch vehicle is high temperature and complex mixture gas. It passes through near the base surface since the flow of the plume under-expands as the flight altitude increases. Therefore, a large amount of heat transfers to the base surface of the vehicle. It is difficult to simulate the plume flow accurately and estimate the rate of heat transfer since the plume flow shows complex phenomena including a shear layer, a plume induced shock and separation, etc. Moreover, In the case of solid propellants Al_2O_3 particles are included in the plume as products of combustion of aluminum. These particles affect the distribution of temperature of the plume and the rate of heat transfer.

Many related researches have been performed by various researchers. Ebrahimi et al. point out a consideration of the turbulent flow, finite-rate chemistry for accurate simulations [1]. Rao et al. analyze influences of turbulent model on plume. Change of turbulent energy causes a few hundred degrees of temperature differences in the shear layer when a two-equation turbulent model is used [2]. As an consideration of non-equilibrium flow effect, Hall et al. compare the four different model, perfect gas, "equivalent" species that is calorically perfect, "equivalent" species that is calorically imperfect and multi-species model with finite-rate chemistry [3]. Burt and Boyd carry out the simulation of flow including Al_2O_3 particles by using direct simulation Monte Carlo (DSMC) method. In the simulation, particle temperature is higher than that of gaseous mixture. And the increase in particle size leads to the increase in the temperature of particle because of difference of heat capacity [4]. According to studies mentioned above, turbulent flow, chemically non-equilibrium flow and gas-particle two phase flows should be considered for accurate simulations of the plume. Also, an

accurate estimation of the heat flux to the base surface requires radiative heat flux as well as convective heat flux.

The objective of this paper is to simulate the base flow with plume and estimate the heat flux to the base surface accurately. Therefore, the simple particle model and the P-1 radiation model are adopted. And consequently influences of the particle size and the flight altitude on the heat flux are investigated.

2 Governing Equation

In the present study a) 2D-axisymmetric non-equilibrium flow, b) kw-SST turbulent flow, c) Al_2O_3 particle model, d) P-1 radiation model are considered. The AUSMPW+ scheme [12] is used for spatial discretization and 3th order Multi-dimensional Limiting Process (MLP3) [13] is used as a limiter. LU-SGS scheme is used for time integration.

The governing equation of non-equilibrium 2D-axisymmetric flow is as follows.

2.1 Non-equilibrium 2D-axisymmetric flows

Two-dimensional axisymmetric Navier-Stokes equation that includes species equations is expressed in Equations (1) and (2).

$$\frac{\partial Q}{\partial t} + \frac{\partial E}{\partial x} + \frac{\partial F}{\partial y} + H = \frac{\partial E_v}{\partial x} + \frac{\partial F_v}{\partial y} + H_v - S_p \quad (1)$$

$$Q = (\rho, \rho u, \rho v, \rho e_t, \rho_i)^T \quad (2)$$

where S_p denotes particle source term which comes from governing equations of Al_2O_3 particle model. CO, CO_2 , Cl, H, H_2 , H_2O , HCl, N_2 , NO, O, OH, O_2 are considered as a species of plume and O, N, NO, O_2 , N_2 as a species of freestream air. JANAF tables [5] are referred for the heat of formations and the molecular weights of species. The mass fractions of species at the nozzle chamber condition is obtained using NASA computer program CEA (Chemical Equilibrium with Applications) [6,7] which calculates chemical equilibrium compositions.

2.1.1 Transport properties

Wilke's mixture rule [8] is employed to calculate mixed gaseous transport properties. Viscosity and thermal conductivity are obtained as Equations (3), (4) and (5).

$$\mu = \sum_s X_s \frac{\mu_s}{\Phi_s}, \quad \kappa = \sum_s X_s \frac{\kappa_s}{\Phi_s} \quad (3)$$

$$X_s = \frac{\rho_s}{\rho} \frac{M}{M_s}, \quad M = \left(\sum_s \frac{c_s}{M_s} \right)^{-1} \quad (4)$$

$$\Phi_s = \sum_i X_i \left[1 + \sqrt{\frac{\mu_s}{\mu_i}} \left(\frac{M_i}{M_s} \right)^{1/4} \right]^2 \left[\sqrt{8} \left(1 + \frac{M_s}{M_i} \right)^{1/2} \right]^{-1} \quad (5)$$

The μ , κ , ρ and M are viscosity, thermal conductivity, density, molecular weight, respectively and subscript i and s means species.

2.2 Turbulent Model

In this study $k\omega$ -SST turbulent model is used since it show good results in sensitivity test and goodness test at mixing layer and round jet which are important parameters in calculating the exhausted plume [14]. The $k\omega$ -SST turbulent model adopts blending function, so this model utilizes the $k\omega$ model in the boundary layer region and switches to the $k\epsilon$ model in the outer region and free shear flow [15].

2.3 Al_2O_3 Particle Model

In the case of solid propellant rocket, aluminum can be used in order to enhance the performance of solid rocket motors. Aluminum which burned under the condition of high temperature and high pressure makes the Al_2O_3 particles. A lot of particles are included in the flow exhausted through the supersonic nozzle because generally aluminum comprise 10 to 30 wt% of total solid propellant. These particles transfer the momentum and energy to the gaseous mixture in the plume. For this reason, considering the Al_2O_3 particles contribute to predict accurate plume structure and the heat flux to the base surface. Moreover, the radiative heat flux of particles takes a large part due to its high temperature

The basic assumptions employed in this research are:

- 1) The volume occupied by the condensed particles is negligible
- 2) Brownian motion of the condensed particles is negligible
- 3) A collision between particles is negligible
- 4) The only forces on the condensed particles are viscous drag forces
- 5) Phase and size change of particles is negligible
- 6) Particles are the sphere and have homogeneous properties
- 7) A diffusion of particle is negligible

Governing equations of Al_2O_3 particles are written in Equations. (6) - (8). Subscript p means particle.

$$\frac{\partial \rho_p}{\partial t} + \frac{\partial \rho_p u_p}{\partial x} + \frac{\partial \rho_p v_p}{\partial y} + \frac{\rho_p v_p}{y} = 0 \quad (6)$$

$$\rho_p \frac{D\vec{V}_p}{Dt} = \frac{\pi D_p^2 \rho C_D}{8m_p} \rho_p |\vec{V} - \vec{V}_p| (\vec{V} - \vec{V}_p) \quad (7)$$

$$\rho_p \frac{DH_p}{Dt} = \frac{Nu_p \pi k D_p (T - T_p)}{m_p} \quad (8)$$

where H is an enthalpy, D_p is a diameter of particle and m_p is a mass of one particle. In this study m_p is $4004.8 \times \left(\frac{1}{6} \pi D_p^3\right)$. Drag coefficient C_D and Nusselt number Nu_p proposed by Hwang [9] are employed in this study.

2.4 P-1 Radiation Model

P-1 radiation model are employed which transforms the radiative transfer equation (RTE) into an elliptical equation. P-1 model can be calculated by the finite volume method, thus it has an advantage in CFD. The simple derivation of P-1 approximation and as a governing equation of P-1 radiation model, transport equation about incident radiation G is introduced.

The complete RTE at position r along the s -direction can be written as

$$\frac{dI_\lambda}{ds} = a_\lambda I_{b\lambda} - (a_\lambda + \sigma_{s\lambda}) I_\lambda + \frac{\sigma_{s\lambda}}{4\pi} \int_0^{4\pi} I_\lambda(s, \omega_i) \Phi(\lambda, \omega_i) d\omega_i \quad (9)$$

where I_λ is the spectral radiation intensity in the unit solid angle ω , a_λ is the absorption coefficient depending on the wavelength λ , $\sigma_{s\lambda}$ is the scattering coefficient, Φ is the spectral scattering phase function, $I_{b\lambda}$ is the spectral black-body intensity and ω_i denotes the solid angle. Radiation intensity can be expressed in terms of a two-dimensional generalized Fourier series as

$$I = \sum_{l=0}^{\infty} \sum_{m=-l}^l I_l^m(r) Y_l^m(\hat{s}) \quad (10)$$

where $I_l^m(r)$ are position-dependent coefficients and $Y_l^m(\hat{s})$ are *spherical harmonics*, given by

$$Y_l^m(\hat{s}) = (-1)^{(m+|m|)/2} \left[\frac{(l-|m|)!}{(l+|m|)!} \right]^{1/2} e^{im\varphi} P_l^{|m|}(\cos\theta) \quad (11)$$

that satisfies Laplace's equation in spherical coordinates. Here θ and φ are the polar and azimuth angle, and $P_l^{|m|}(\cos\theta)$ are *associated Legendre polynomials* [10]. It is known as P-N model in the case of $l=N$

Equations (10) may be written in P-1 model as

$$I(r, \hat{s}) = \frac{1}{4\pi} [G(r) + 3q(r) \cdot \hat{s}] \quad (12)$$

Then, substituting equation (12) into equation (9) and integrating over all solid angles leads to

$$\nabla I \nabla G - aG + 4\sigma T^4 = 0 \quad (13)$$

where G is incident radiation, σ denotes Stefan–Boltzmann constant and $\Gamma = 1/(3a)$.

Equation (13) is a governing equation of P-1 radiation model. In this equation, scattering term is neglected.

Thermal radiation term that appears in the gas dynamic energy equation is obtained using incident radiation G in Equation (14).

$$\nabla \cdot q_{rad} = \kappa(-G + 4\sigma T^4) \quad (14)$$

Wall boundary conditions for solving Eq. (13) are:

- 1) Dirichlet condition

$$G_w = 0 \quad (15)$$

- 2) Marshak condition

$$\frac{1}{\kappa} \nabla G \cdot \hat{n} = -\frac{3}{2} \frac{\varepsilon_w}{(2 - \varepsilon_w)} G \quad (16)$$

where ε_w is emissivity of wall and in this study $\varepsilon_w = 0.5$.

3 Results and Discussion

3.1 Plume Structure according to Flight Altitude

3.1.1 Flow conditions & grid system

A numerical simulation of the plume flow field and estimation of the heat flux to the base surface are conducted at altitude of 10km and 50km. Particle model and P-1 radiation model are not considered. Figure 1 is the rocket configuration and grid system which are studied in this research. The basic rocket configuration is 15° nose cone and cylinder shape body without a nozzle lip [16]. Nozzle is designed to make exit Mach number be 3.0 based on the assumption of ideal gas and divergent part of nozzle has conical shape. The angle of nozzle exit is about 18.435° .

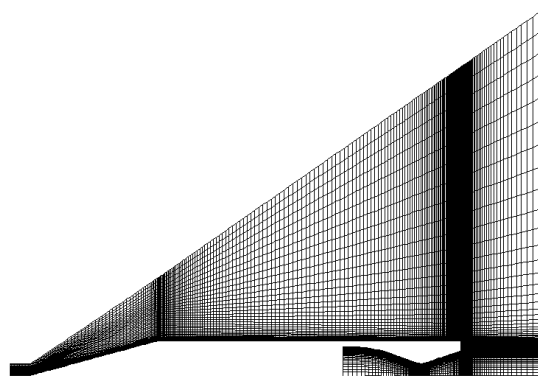
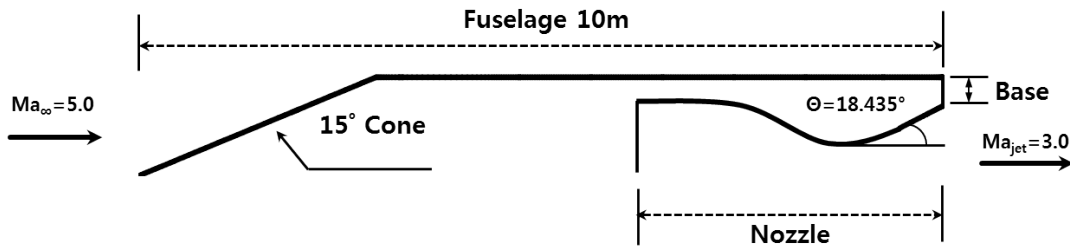


Figure 1 Rocket configuration and grid system

Table 1 Freestream conditions

	Case 1	Case 2
Altitude [km]	10	50

Mach number	5.0	5.0
Pressure [pa]	26500	79.779
Temperature [K]	223.25	270.65
Reynolds number	4.27×10^8	1.01×10^6
Wall temperature [K]	600	

Freestream conditions and chamber conditions are shown in table 1 and Table 2, respectively. As an initial condition in the nozzle, composition of plume species is obtained using CEA code developed by NASA Glenn Research Center. It is assumed that APCP (Ammonium perchlorate composite propellant) is a solid propellant.

Table 2 Chamber conditions & propellants

Total pressure [bar]	70
Total temperature [K]	3000
Propellants	Al, C ₄ H ₂ , NH ₄ ClO ₄ (I)

Species which have mole fraction under the 2×10^{-4} are neglected. As a result, following species are decided as a chemical composition of plume.

Table 3 Plume species and properties

Species	Molecular weight	Heat of formation (J/kmole $\times 10^8$)	Mass fraction
O	15.9994	2.49170	2.482×10^{-4}
N	14.0067	4.72680	0.000
H	1.0079	2.17999	1.641×10^{-4}
Cl	35.4530	1.21302	1.338×10^{-2}
OH	17.073	0.38987	5.816×10^{-3}
H ₂	2.0159	0.00000	4.059×10^{-3}
CO	28.0104	-1.10530	1.832×10^{-1}
HCl	36.4609	-0.92312	2.512×10^{-1}
NO	30.0061	0.90291	1.263×10^{-3}
O ₂	31.9988	0.00000	1.146×10^{-3}
N ₂	28.0134	0.00000	1.012×10^{-1}
H ₂ O	18.0153	-2.41826	2.116×10^{-1}
CO ₂	44.0098	-3.93522	2.268×10^{-1}

3.1.2 Plume structure and heat flux

In both 10km and 50km, flow is under-expanded since pressure ratio $p_{\text{exit}}/p_{\text{back}}$ is about 6 at 10km and 1850 at 50km. The pressure ratio affects the location of flow separation. Separation induced by interaction between plume and air are shown in Figure 2, 3. At altitude 10km separation is developed near the base surface and at altitude 50km separation is shown in the rear fuselage.

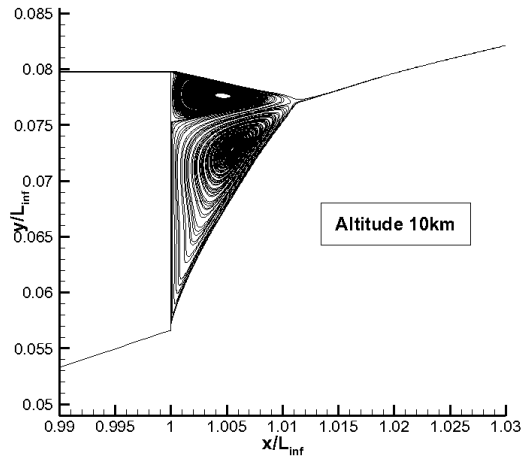


Figure 2 Separation at 10km

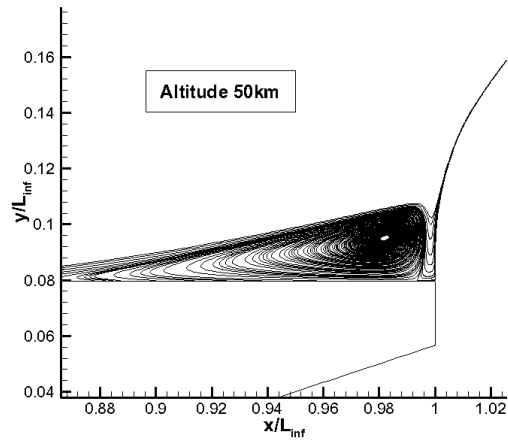


Figure 3 Separation at 50km

Figure 4 shows the heat flux to the base surface according to altitude. The x axis denotes non-dimensionalized radial distance from centerline of the nozzle at base surface. In both cases sharp increase of the heat flux at nozzle exit are shown. The heat flux at altitude of 10km is higher than at altitude of 50km. Except for the values near the nozzle exit, averaged heat flux at altitude of 10km is about $1.18 \times 10^5 \text{ W/m}^2$ and at altitude of 50km is about $6.38 \times 10^4 \text{ W/m}^2$. This is because density at 10km is higher than at 50km. In the case of 10km, the heat flux is high at near 0.075 which is the stagnation point as shown in Figure 2. This is the characteristic of $k\omega$ -SST turbulent model which appears high value at stagnation point and low value at the other region in the heat flux. However averaged heat flux of this model is reasonable compare to DES or LES results.

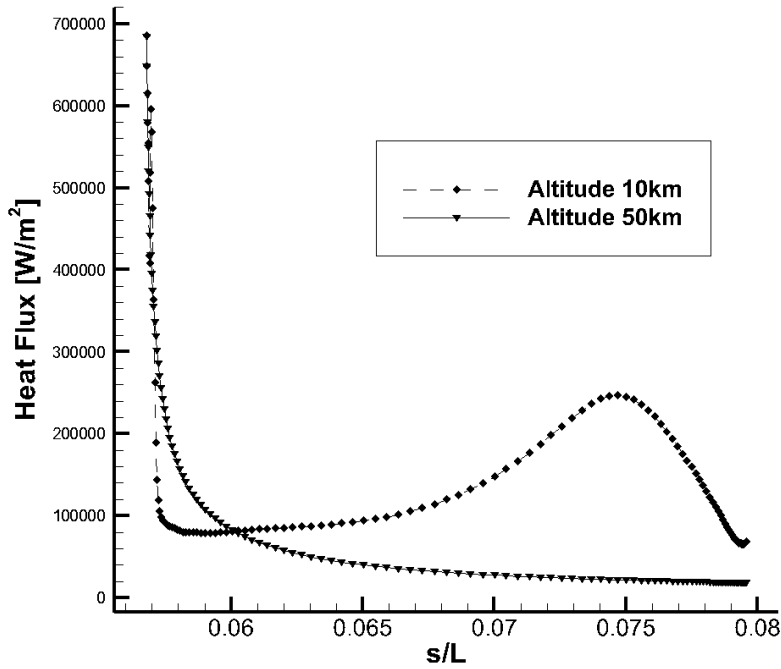


Figure 4 Heat fluxes to base surface according to altitude

3.2 Al₂O₃ Particle Flow Field according to Particle Size

3.2.1 Flow conditions & Grid system

The effect of particles according to the particle size is investigated. Freestream conditions are case 1 of table 3 and chamber conditions are written in table 4. Figure 5 is the closer look of nozzle grid system.

Table 1 Inflow conditions in nozzle

T ₀ [K]	3000
P ₀ [bar]	70
Re#	4.27×10 ⁸
Particle radius [μm]	1, 5, 10, 20
Particle wt%	30

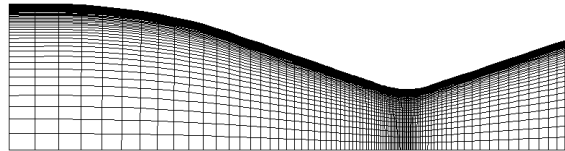
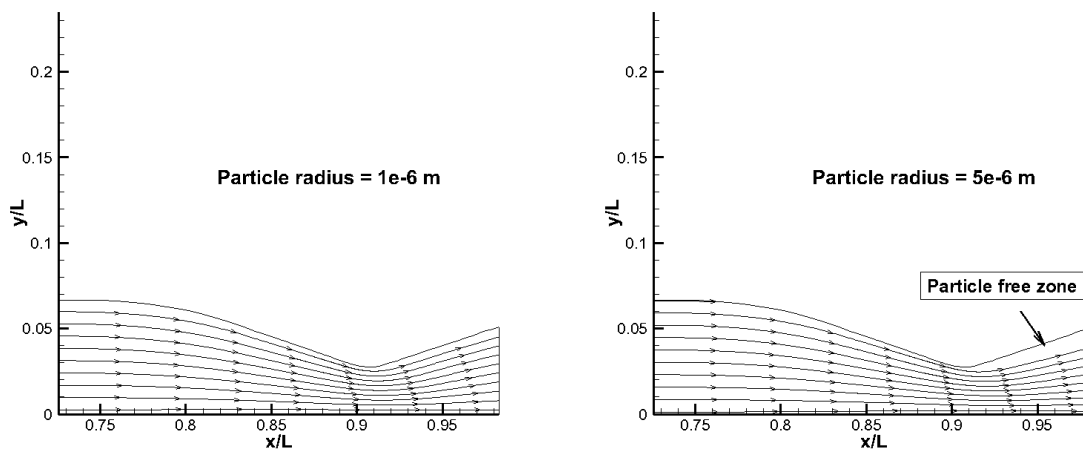


Figure 5 Grid system of the nozzle

3.2.2 The motion of particles in the nozzle

Fig. 6 appears streamlines of particles in the nozzle. Small particles more easily follow the flow of the gaseous mixture. And big particles concentrate on the centerline of the nozzle because of inertial force. In other words, small particles more interact with gaseous phase than big particles because particle source terms S_p is proportional to $1/D_p$ or $1/D_p^2$. Also, drag coefficient is increased as particle size is decreased. As a result, particle free zone is appeared in the divergent part of nozzle. The particle free zone expands as the size of particle is increased.



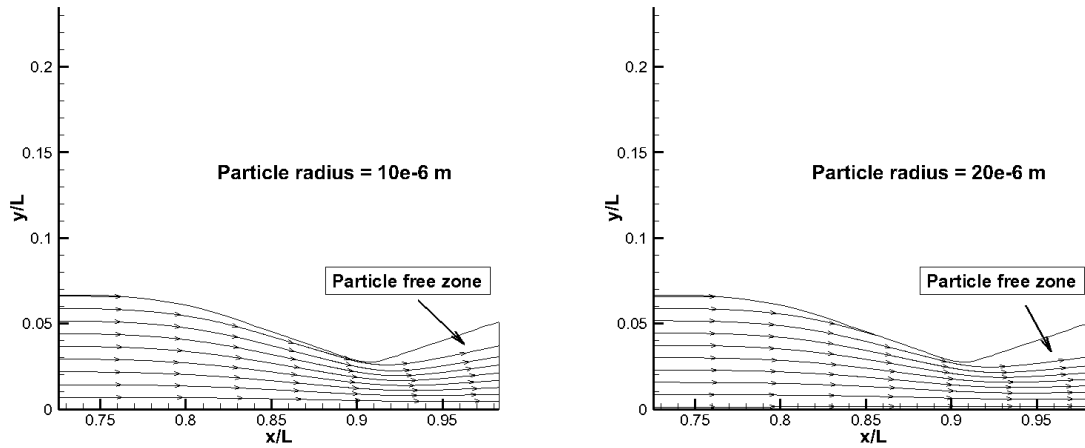


Figure 6 Streamlines of particles

And the distribution of particles are also affected by the radius of curvature at nozzle throat. When the area of nozzle changes steeply, particles move while maintaining their direction and finally concentrate more on the centerline.

3.2.3 Temperature and velocity lag

Figure 7 and 8 shows temperature and velocity distribution at nozzle exit, respectively. Temperature and velocity lag between the gas phase and the particle phase becomes large when the particle size becomes big. This is also because small particles more interact with gas phase than big particles. The velocity of particles is slower than the velocity of gas. The temperature is contrary. Therefore, the particle phase transfers thermal energy to the gas phase and takes kinetic energy away from the gas phase.

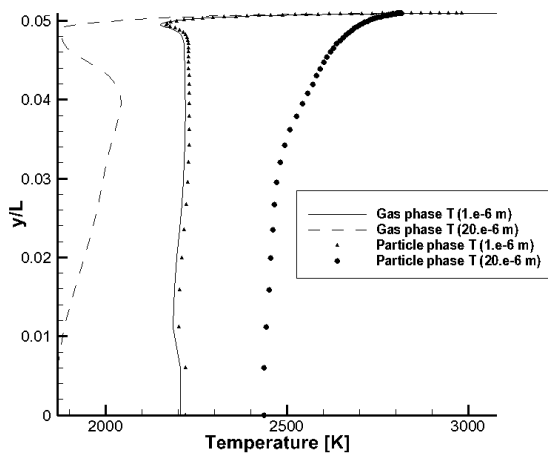


Figure 7 Temperature lags at nozzle exit

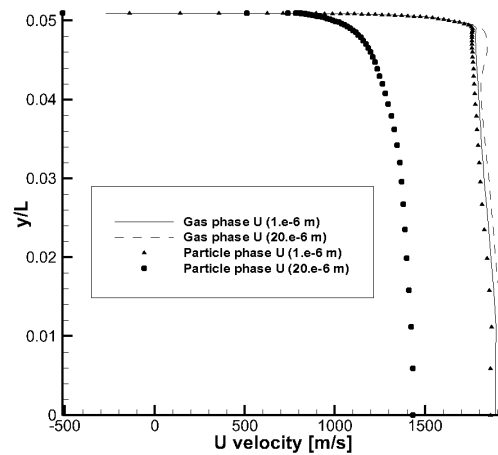


Figure 8 Velocity lags at nozzle exit

3.2.4 Change of the heat flux according to particle size

Figure 9 is temperature distribution of gas phase at nozzle exit according to particle size. *One Phase* denotes the case of no particles. The temperature is increased when particles are considered. This is because total enthalpy of two-phase is larger than the one-phase. Averaged temperature at nozzle exit is increased as particle size is decreased. Moreover, temperature of gas phase is lower in the particle

free zone than in the other region. When the radius of particle is $1\mu\text{m}$, particle free zone is the smallest and temperature is higher than other cases relatively.

The temperature at nozzle exit influences on the heat flux to the base surface. Heat fluxes according to particle size are shown in Figure 10. The heat flux becomes large as the size of particle becomes small. Especially, in case of particle of $1\mu\text{m}$ radius of which case does not have particle free zone, the heat flux is much higher than other cases.

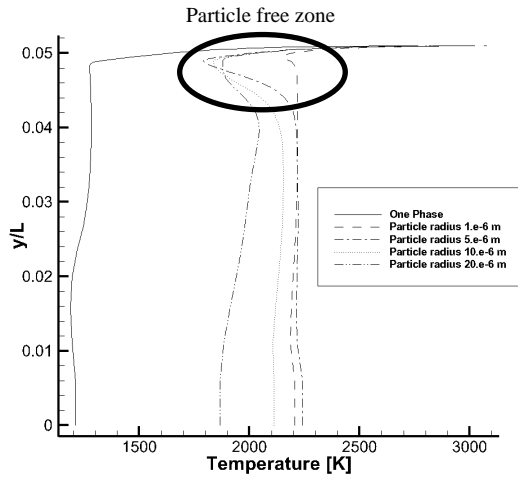


Figure 9 Temperature distribution at nozzle exit

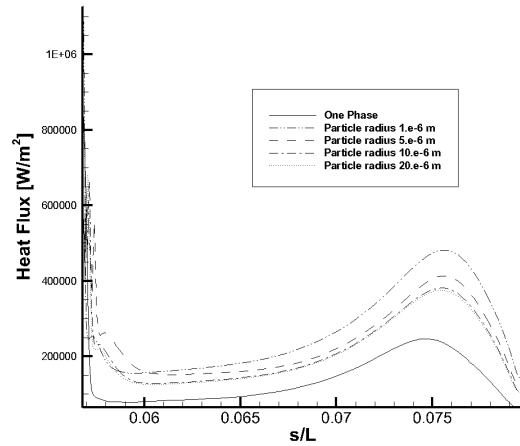


Figure 10 Heat Fluxes according to particle size

3.3 Effect of P-1 radiation model

3.3.1 Flow conditions and absorption coefficients

Numerical analysis about the rocket configuration of Figure 1 is carried out to study the effect of P-1 radiation model on the heat flux to the base surface. Freestream conditions and chamber conditions are same as table 1, 3, 4. Gauss-Seidel iteration method is used to calculate P-1 radiation model. As a wall boundary condition Marshak condition of Eq. (16) is applied.

CO_2 , H_2O , CO , HCl , NO and Al_2O_3 are considered in absorption coefficients. Simple total absorption coefficient, known as Plank-mean absorption coefficient is used except Al_2O_3 particle. Figure 11 shows Plank-mean absorption coefficient of these species according to temperature [10].

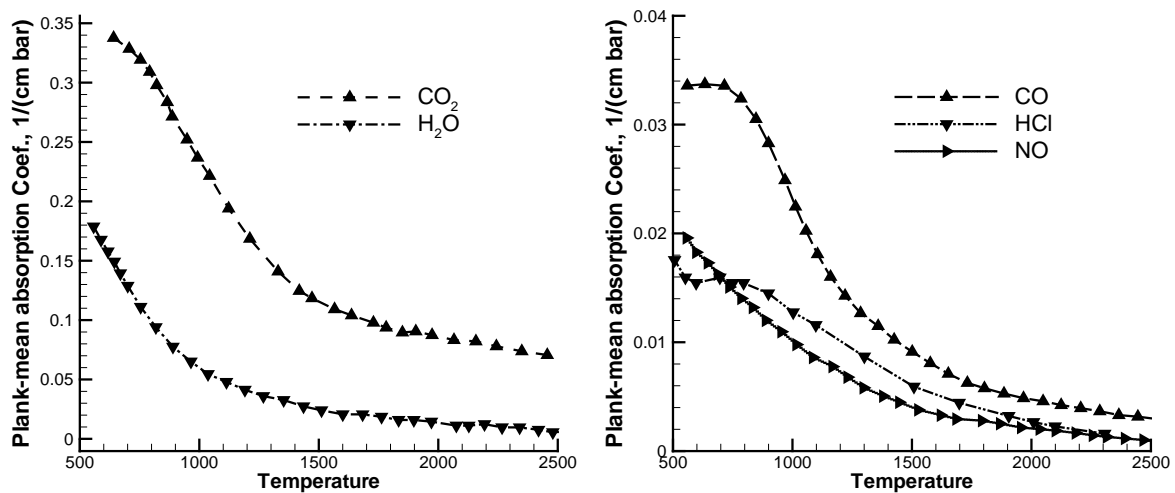


Figure 11 Plank-mean absorption coefficients

3.4.2 The radiative heat flux without particles according to altitude

At the same altitude, convective heat fluxes are same since temperature gradient at the wall is little changed. Therefore a difference of the total heat flux is only determined by radiative heat flux. Figure 12 shows radiative heat fluxes at altitude of 10km and 50km. Averaged radiative heat flux at altitude of 10km is $3.96 \times 10^4 \text{ W/m}^2$ and at altitude of 50km is $4.00 \times 10^4 \text{ W/m}^2$. The radiative heat flux values are almost same regardless of altitude.

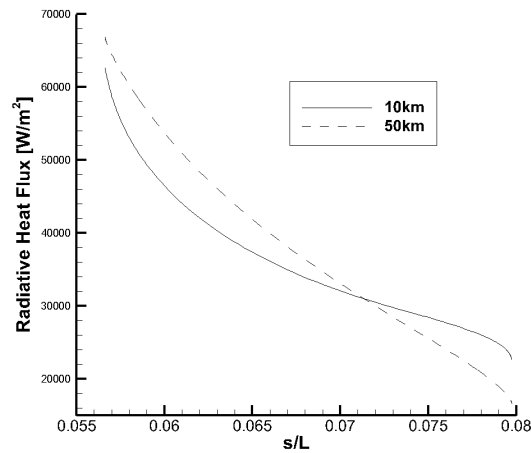


Figure 12 Radiative heat fluxes according to altitude

4 Conclusion and Future Work

The effects of Al_2O_3 Particle on convective and radiative heat flux to rocket base Surface are studied. Simple particle equation is introduced and P-1 radiation model is adopted. The convective heat flux is increased as flight altitude is decreased. Also, convective heat flux is increased as particle size is decreased. The radiative heat flux is increased as the size of particle is decreased, on the other hand, it is less sensitive to flight altitude. In the future work, discrete ordinate method would be employed as a radiation model. The investigation of comparison between P-1 radiation model and discrete ordinate method would be carried out.

References

- [1] H. B. Ebrahimi, J. Levine, and A. Kawasaki, "Numerical Investigation of Twin-Nozzle Rocket Plume Phenomenology", *Journal of Propulsion and Power*, Vol.16, No. 2, 2000, pp. 178-186.
- [2] R. M. Rao, K. Sinha, G. V. Candler, M. J. Wright and D. A. Levin, "Numerical Simulations of Atlas II Rocket Motor Plumes", 35th AIAA/ASME/SAE/ASEE Joint Propulsion Conference and Exhibit, June 20 - 23, 1999, Los Angeles, CA.
- [3] L. Hall, M. P. Applebaum and W. M. Eppard, "Multi-species Effects for Plume Modeling on Launch Vehicle Systems", 49th AIAA Aerospace Sciences Meeting including the New Horizons Forum and Aerospace Exposition, 4 - 7, January, 2011, Orlando, Florida.
- [4] J. M. Burt and I. D. Boyd, "High Altitude Plume Simulations for a Solid Propellant Rocket", 45th AIAA Aerospace Sciences Meeting and Exhibit, Reno, Nevada, 8 - 11, January, 2007.
- [5] M. W. Chase, "NIST-JANAF Thermochemical Tables 4th Edition", *Journal of Physical and Chemical Reference Data*.
- [6] S. Gordon and B. J. McBride, "Computer Program for Calculation of Complex Chemical Equilibrium Compositions and Applications I. Analysis", NASA Reference Publications 1311, October 1994
- [7] S. Gordon and B. J. McBride, "Computer Program for Calculation of Complex Chemical Equilibrium Compositions and Applications II. Users Manual and Program Description", NASA Reference Publications 1311, June 1996
- [8] C. R. Wilke, "A Viscosity Equation for Gas Mixtures", *The Journal of chemical Physics*, Vol.18, No.4, 1950.
- [9] C. J. Hwang and G. C. Chang, "Numerical Study of Gas-Particle Flow in a Solid Rocket Nozzle", *AIAA Journal*, Vol.26, No.6, pp.682-689, 1998.
- [10] M. F. Modest, "Radiative Heat Transfer", The Pennsylvania State University.
- [11] S. S. Sazhin, E. M. Sazhina, O. Faltsi-Saravelou and P. Wild, "The P-1 Model for Thermal Radiation Transfer: advantages and limitations", *Fuel*, Vol.75, No.3, pp.289-294, 1996.
- [12] K. H. Kim, C. Kim and O. Rho, "Methods for the Accurate Computations of Hypersonic Flows – Part I AUSMPW+ Scheme", *Journal of Computational Physics*, Vol.174, No.1, pp.38-80 2001.
- [13] K. H. Kim, C. Kim, "Accurate, Efficient and Monotonic Numerical Methods for Multi-dimensional Compressible Flows Part II: Multi-dimensional Limiting Process", *Journal of Computational Physics*, Vol.208, No.2, pp.570-615, 2005.
- [14] J. E. Bardina, P. G. Huang and T. J. Coakley, "NASA TM 110446", 2997.
- [15] F. R. Menter, "Two-equation Eddy-Viscosity Turbulence Models for Engineering Applications", *AIAA Journal* Vol.32, No.8, 1994.
- [16] R. J. McGhee, "Jet-Plume-Induced Flow Separation on Axisymmetric Bodies at Mach Numbers of 3.00, 4.50 and 6.00", NASA TM X-2059.